LHCb-PAPER-2014-051
supplementary material

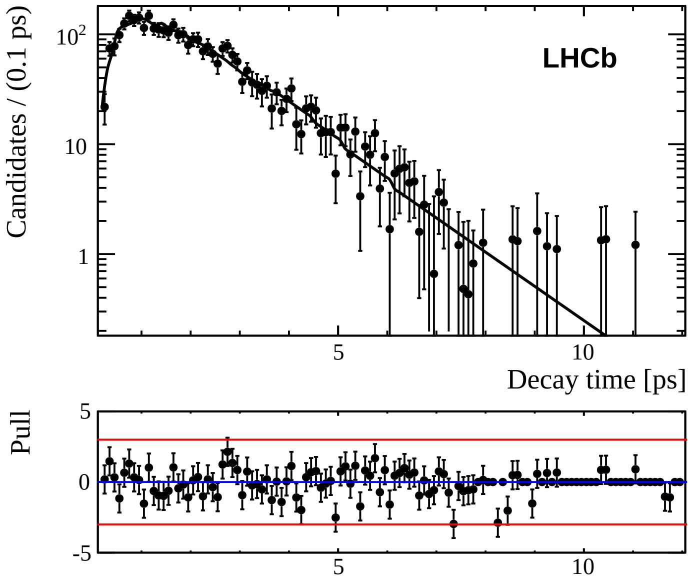

Figure 1: Decay time distribution as per Fig.4 with pull distribution included.

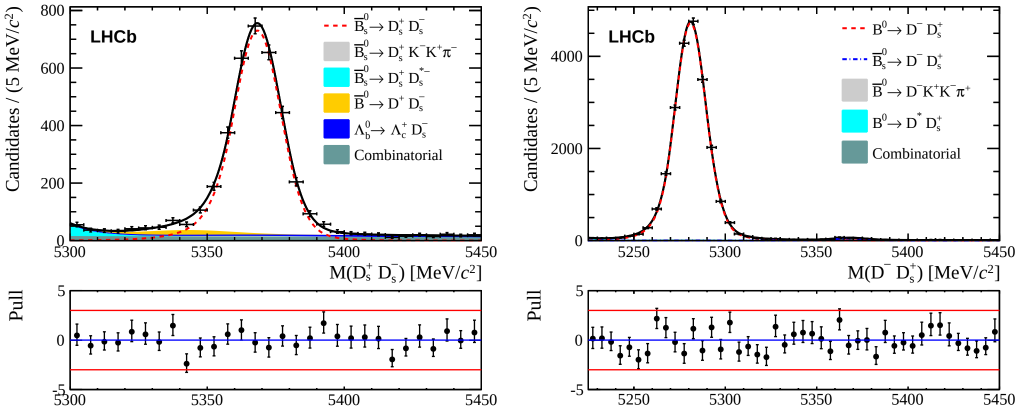

Figure 2: Mass distributions as per Fig.1 with pull distributions included.

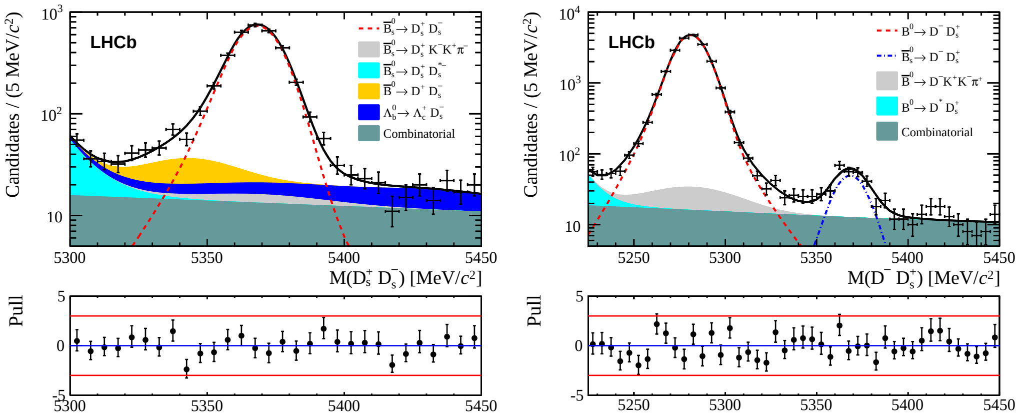

Figure 3: Mass distributions as per Fig.1 on a logarithmic scale, with pull distributions included.

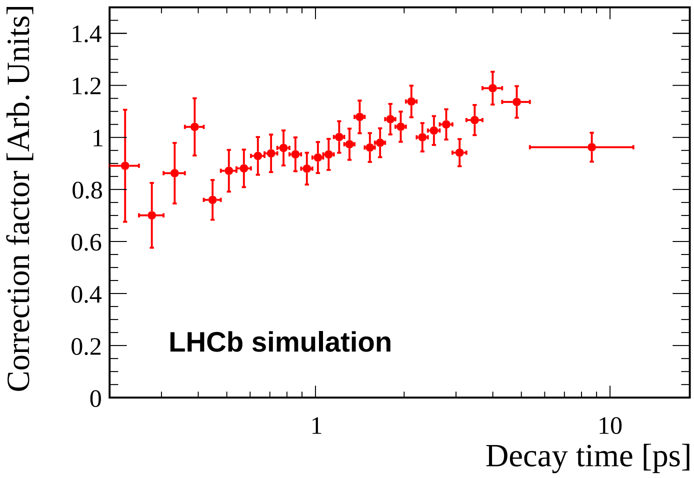

Figure 4: Correction factor between simulated $D_s^+D_s^-$ and $D^-D_s^+$ acceptances. This is the correction applied to the $D^-D_s^+$ data-driven acceptance in Fig. 2(a), green, in order to obtain Fig. 2(b), red.

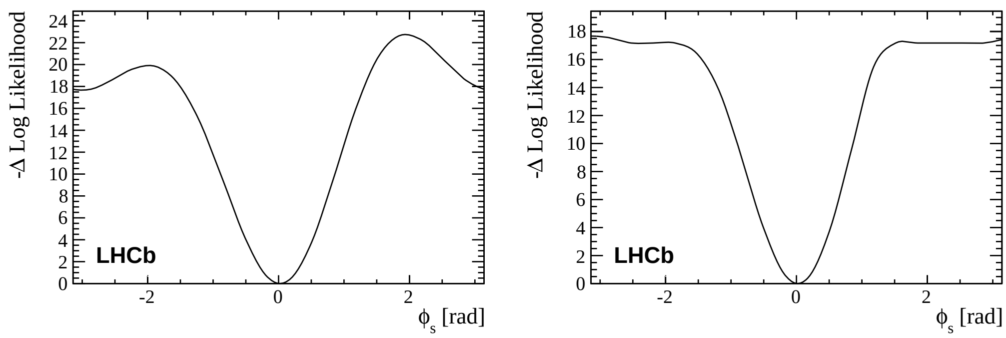

Figure 5: Profile likelihood of ϕ_s for the $|\lambda| = 1$ fit (top) and the floated $|\lambda|$ fit (bottom) in data.

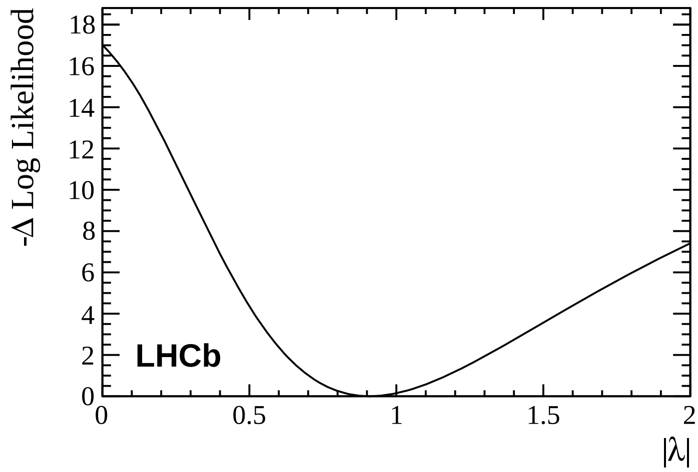

Figure 6: Profile likelihood of $|\lambda|$ in data.

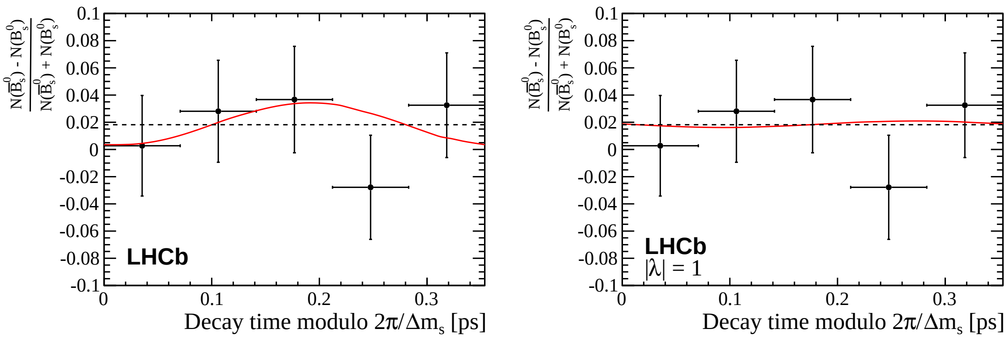

Figure 7: The raw asymmetry distributions with fits overlaid. The offset is due to a difference in the number of $\bar{B}^0_s$ and B^0_s tags, which corresponds to an asymmetry in the tagging efficiency that is, however, consistent with zero. On top is the case where $|\lambda|$ is a free parameter. The flavour tagging calibration has been applied to the data, rather than as part of the fit as is the case in the fits to extract ϕ_s.

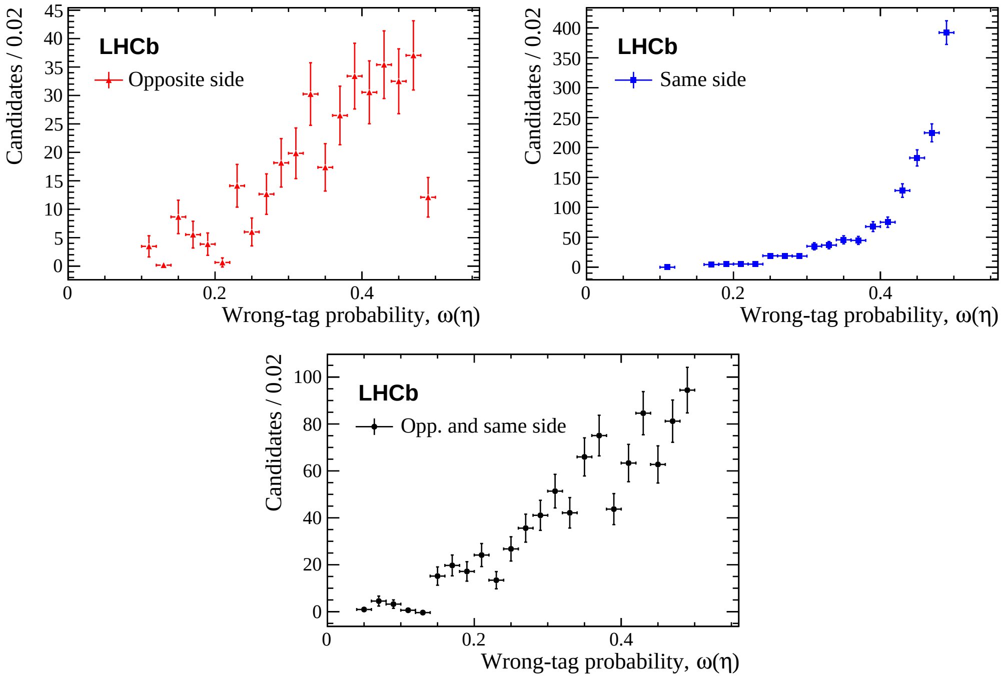

Figure 8: Calibrated wrong-tag *sPlot* distributions in data. The three tagging categories are shown: Candidates with an opposide-side tag only are shown in red, while candidates with a neural-net same-side kaon tagger only are shown in blue. Candidates with both OS and SSK tags have a combined wrong-tag probability as shown in black.

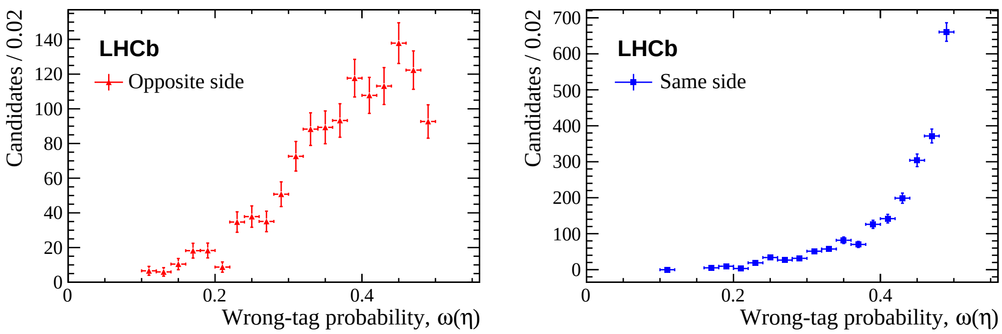

Figure 9: Inclusive calibrated wrong-tag *sPlot* distributions in data. The two tagging categories are shown: All candidates with an opposide-side tag are shown in red, while candidates with a neural-net same-side kaon tag are shown in blue.

Table 1: Inclusive performance of the tagging algorithms used in this analysis, post calibration. The tagging values are determined for events where this tagger makes a decision inclusively, *i.e.*: whether or not the other tagger makes a decision.

	OS Cut-based	SSK Neural-net
Tagging efficiency, ϵ	$(39.18 \pm 0.85)\%$	$(70.53 \pm 0.80)\%$
Effective wrong-tag prob., ω_{eff}	$0.3508 \pm 0.0015 \pm 0.0037$	$0.4084 \pm 0.0045 \pm 0.0035$
Effective tagging power $\epsilon D^2_{\text{eff}}$	$(3.49 \pm 0.10 \pm 0.17)\%$	$(2.37 \pm 0.23 \pm 0.18)\%$
Combined $\epsilon D^2_{\text{eff}}$	$(5.33 \pm 0.18 \pm 0.17)\%$	

Table 2: Exclusive performance of the tagging algorithms used in this analysis, post calibration. The exclusive tagging values are determined for events where only this tagger makes a decision. The Overlap values are determined for events where both tagging algorithms make a decision.

	OS Cut-based	SSK Neural-net
Excl. tagging eff., ϵ	$(10.66 \pm 0.54)\%$	$(40.02 \pm 0.86)\%$
Excl. effective wrong-tag prob., ω_{eff}	$0.3405 \pm 0.0016 \pm 0.0039$	$0.4057 \pm 0.0046 \pm 0.0036$
Excl. effective tagging power $\epsilon D^2_{\text{eff}}$	$(1.08 \pm 0.06 \pm 0.05)\%$	$(1.42 \pm 0.46 \pm 0.36)\%$
Overlap ϵ	$(26.51 \pm 0.77)\%$	
Overlap ω_{eff}	$0.3367 \pm 0.0016 \pm 0.0033$	
Overlap $\epsilon D^2_{\text{eff}}$	$(2.83 \pm 0.10 \pm 0.11)\%$	
Combined $\epsilon D^2_{\text{eff}}$	$(5.33 \pm 0.18 \pm 0.17)\%$	

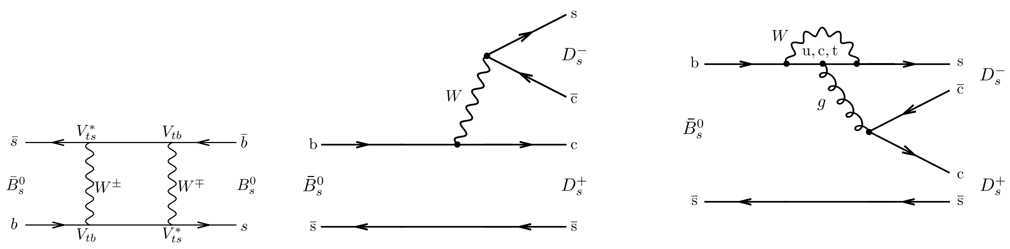

Figure 10: Diagrams pertinent to $\overline{B}{}^0_s \to D_s^+ D_s^-$. Left: $\overline{B}{}^0_s$-B_s^0 mixing. Centre: $\overline{B}{}^0_s \to D_s^+ D_s^-$ tree, Right: $\overline{B}{}^0_s \to D_s^+ D_s^-$ penguin.

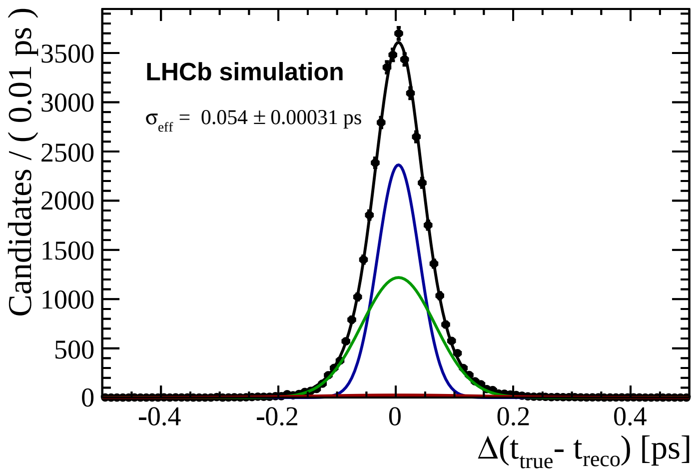

Figure 11: Effective resolution determination in simulated signal candidates. A triple-Gaussian is overlaid. The effective resolution is the fractional weighted quadrature sum of the widths of the three Gaussians.

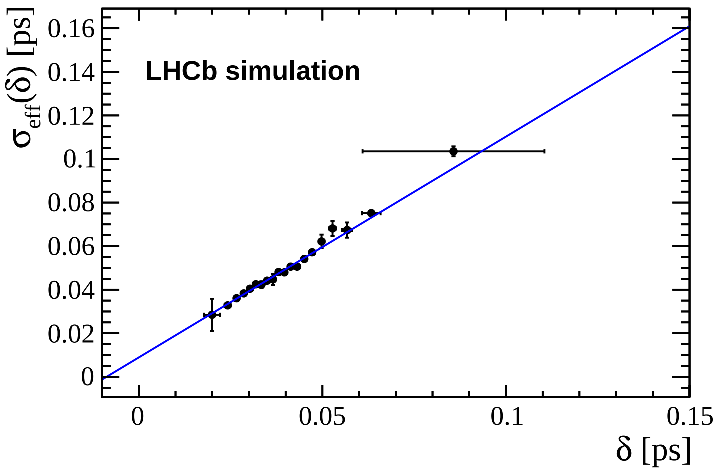

Figure 12: Effective resolution as a function of the per-event decay time error. A linear χ^2 fit is overlaid, in which both horizontal and vertical uncertainties are taken into account.